

Quantum Dynamics of a Hydrogen Molecule Inside an Anisotropic Open-Cage Fullerene: Coupled Translation-Rotation Eigenstates and Comparison with Inelastic Neutron Scattering Spectroscopy[†]

Shufeng Ye,[§] Minzhong Xu,[§] Zlatko Bačić,^{*,‡,§} Ronald Lawler,[†] and Nicholas J. Turro^{*,†}

State Key Laboratory of Precision Spectroscopy and Department of Physics, Institute of Theoretical and Computational Science, East China Normal University, Shanghai 200062, China, Department of Chemistry, New York University, New York, New York 10003, Department of Chemistry, Brown University, Providence, Rhode Island 02912, and Department of Chemistry, Columbia University, New York, New York 10027

Received: May 13, 2010; Revised Manuscript Received: June 25, 2010

We report rigorous quantum five-dimensional (5D) calculations of the translation-rotation (T-R) energy levels and wave functions of H₂ inside aza-thia-open-cage fullerene (ATOCF). Translational and rotational excitations of this endohedral complex have been measured in a recent inelastic neutron scattering (INS) study, enabling direct comparison between theory and experiment. ATOCF has no symmetry, and therefore the intermolecular potential energy surface (PES) governing the T-R dynamics of H₂ is strongly anisotropic. A pairwise additive PES is employed in the calculations. Inspection of the wave functions shows three regular quasi-1D translational modes aligned with the Cartesian *x*, *y*, and *z* axes, respectively. These and other translational excitations can be assigned with the Cartesian quantum numbers V_x, V_y, and V_z. The radial anisotropy of the cage environment causes the splitting of the translational fundamental into three excitations whose frequencies differ substantially; the *z* mode directed toward the ATOCF orifice has the lowest frequency and is the most anharmonic. All three translational modes exhibit negative anharmonicity. The *j* > 1 rotational level of H₂ is also split into a triplet, due to the angular anisotropy of the cage. The complete lifting of the degeneracies of the translational fundamental and the *j* > 1 triplet of the encapsulated H₂ molecule that emerges from the calculations is also observed in the INS spectra of H₂@ATOCF. The calculated magnitudes of both splittings, as well as the energies of the individual sublevels, rotational and translational, are in good agreement with the INS data.

I. Introduction

In the past several years, a number of fascinating complexes have been synthesized where the simplest and the most quantum mechanical of molecules, H₂, is encapsulated in a fullerene cage utilizing the “molecular surgery” approach.^{1–3} Among them is the endohedral complex of H₂ with aza-thia-open-cage fullerene (ATOCF),⁴ denoted H₂@ATOCF. ATOCF has a 13-membered orifice containing sulfur and nitrogen atoms (the structure is shown in Figure 1), which was closed by a further set of organic reactions with the H₂ molecule inside the cage, resulting in the elegant, highly symmetric complex H₂@C₆₀.^{5,6} Recently, an open-cage C₇₀ derivative with not just one but also two H₂ molecules trapped in its interior was prepared.⁷ Its orifice was subsequently closed,⁸ thereby completing the synthesis of H₂@C₇₀ (97%) and (H₂)₂@C₇₀ (3%).

The availability of the endohedral fullerene complexes with molecular hydrogen in macroscopic quantities has enabled the investigations of various aspects of the behavior of H₂ molecule(s) encapsulated in fullerene cages. NMR spectroscopy has been employed to probe the dynamics of H₂ in ATOCF^{9,10} and in C₆₀;^{10,11} it has also revealed the positional exchange of two H₂ molecules trapped inside an open-cage C₇₀.⁷ The ability of H₂ in C₆₀ to communicate with the outside world, as measured

by the quenching of ¹O₂ outside the cage,¹² the spin-lattice relaxation rates,¹³ and the interconversion of *para*-hydrogen (*p*-H₂) and *ortho*-hydrogen (*o*-H₂),¹⁴ has been studied in the past couple of years.¹⁵

Endohedral H₂-fullerene complexes present a unique opportunity for experimental and theoretical explorations of the quantum dynamics of a light molecule confined in nanospaces whose geometries are known accurately, and which differ in both size and symmetry. Confinement results in the quantization of the translational motions of the hydrogen molecules, in addition to their quantized rotations. The discrete translational levels are well separated in energy, since H₂ is light and the confining cavities are small. The quantized rotational levels of H₂ are widely spaced as well, on the account of its exceptionally large rotational constant. The translational and rotational degrees of freedom of the guest molecule are coupled, and the resulting translation-rotation (T-R) energy level structure is sparse. Consequently, the T-R, or “rattling”, dynamics of the encapsulated hydrogen molecule is inherently highly quantum mechanical. The large quantum effects are enhanced further by the fact that for the homonuclear isotopologues H₂ and D₂ the symmetry constraints on the total wave function lead to the existence of two distinct species, one having only even-*j* rotational states, *p*-H₂ and *o*-D₂, and the other with exclusively odd-*j* rotational states, *o*-H₂ and *p*-D₂.

The symmetry of the nanocage has a strong influence on the quantum T-R dynamics of the guest hydrogen molecule. It manifests in characteristic patterns of degeneracies of the T-R energy levels, the choice of quantum numbers appropriate for

[†] Part of the “Reinhard Schinke Festschrift”.

* To whom correspondence should be addressed. E-mail: zlatko.bacic@nyu.edu (Z. B.), njt3@columbia.edu (N. J. T.).

[‡] East China Normal University.

[§] New York University.

[†] Brown University.

[‡] Columbia University.

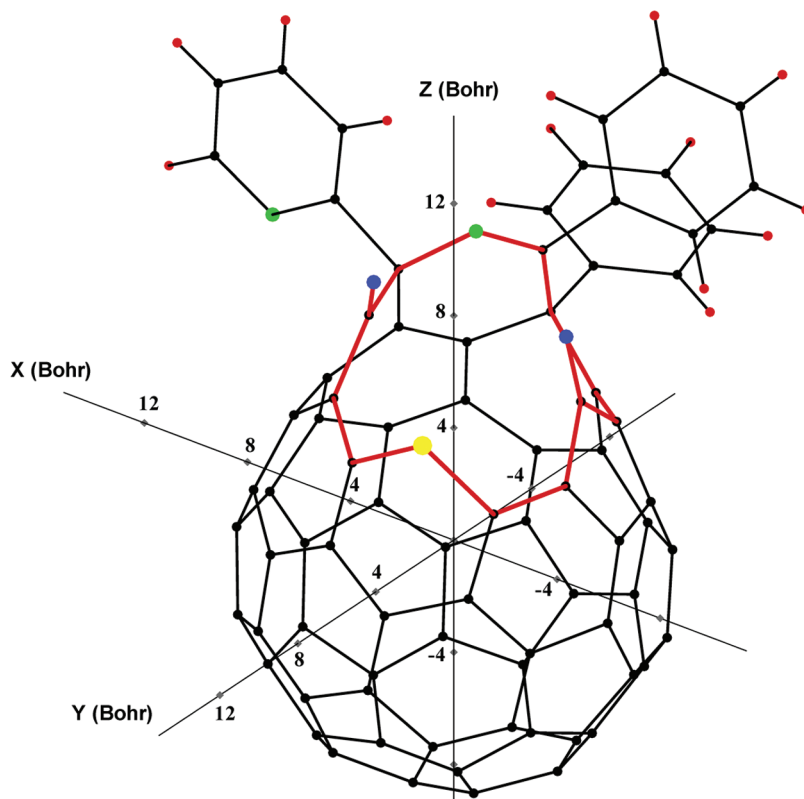


Figure 1. The geometry of ATOFC determined by X-ray crystallography.²⁵ The noncarbon atoms are shown in color: N (green), O (blue), S (yellow), and H (red). Also shown are the principal axes of the molecule.

the assignment of the translational excitations, and the type of coupling between the angular momenta associated with the translational and rotational motions, respectively, all of which depend on the cage symmetry. This link between the symmetry of the confining nanospace and the key features of the T-R dynamics of the guest molecule was illuminated first by our quantum five-dimensional (5D) calculations of the T-R eigenstates of H₂ inside the small^{16,17} and large cages^{18,19} of the structure II (sII) clathrate hydrates. Unlike the carbonaceous fullerenes, these cages are formed by a 3D framework of hydrogen-bonded water molecules, but their dimensions are comparable to those of the fullerenes. It was only natural to extend our investigations to the endohedral H₂-fullerene complexes. The first endohedral complex that we studied was that of H₂ in C₆₀, whose icosahedral (*I*_h) symmetry makes it the most symmetric of all fullerenes. Our quantum 5D calculations of the T-R energy levels of H₂@C₆₀ (refs 20 and 21) revealed an intriguing pattern of degeneracies. These were fully understood in terms of two key features:²⁰ (i) the orbital angular momentum **I** of the center of mass (com) of H₂ and the rotational angular momentum **j** of H₂ couple to give the total angular momentum $\rightarrow \mathbf{I} + \mathbf{j}$, which ranges from $|l| + j$ to $|l| - |j|$ in steps of one; (ii) the integer values of l are those allowed for the quantum number n of the 3D isotropic harmonic oscillator (HO) ($l \leq n, n - 2, \dots, 1$ or 0 , for odd or even n , respectively), which labels in part the translational excitations of H₂ in C₆₀. The T-R levels predicted by this coupling scheme were observed in the recently measured infrared (IR) spectra of H₂@C₆₀.²² These IR spectra made it possible for us to develop and refine the novel three-site H₂-C pair potential.²³ The pairwise additive 5D intermolecular potential energy surface (PES) of H₂@C₆₀ constructed using this two-body potential and the optimal values of its three parameters, when employed in the fully coupled quantum bound-state calculations, reproduced all six T-R energy

levels observed so far in the IR spectra of this endohedral complex to within 1–2 cm⁻¹ (0.6%) or better.²³

The endohedral fullerene complex whose quantum dynamics we investigated next was H₂@C₇₀ (ref 23). The symmetry of C₇₀, D_{5h}, is appreciably lower than that of C₆₀; C₇₀ has a long axis (*z*), coinciding with its C₅ axis of rotation, which is distinct from the two symmetrically equivalent short axes (*x* and *y*, respectively) perpendicular to the C₅ axis. As a result, the intermolecular potential energy surface (PES) of H₂@C₇₀ exhibits a pronounced anisotropy with respect to the direction of the translational motion of the com of H₂ inside the cage. Lowering the symmetry of the environment gives rise to the T-R energy level structure which differs qualitatively from that of H₂@C₆₀, and requires an entirely different set of quantum numbers for its assignment. The translational excitations of H₂ in C₇₀ were assigned in terms of the quantum numbers (V, l) of the 2D isotropic HO associated with the short *x* and *y* axes, where V and l denote the number of quanta in the 2D *xy* mode and the vibrational angular momentum parallel to the *z* axis, respectively, together with the Cartesian quantum number V_z for the 1D translational mode in the *z* direction.

In this paper, we report the results of the quantum 5D calculations of the T-R energy levels and wave functions of the endohedral complex of H₂ in ATOFC. We chose this fullerene because its cage has no symmetry elements. Therefore, it represents the next, and last, logical step of our investigations of the ways in which the quantum T-R dynamics of the encapsulated H₂ is affected by systematically decreasing the cage symmetry: (1) in C₆₀, the three (principal) axes are equivalent (spherical top), and so are the 1D profiles of the 5D intermolecular PES along them; (2) C₇₀ has two axes that are equivalent, and the third is distinct (symmetric top); and the same holds for the 1D cuts through the 5D PES along them; (3) in ATOCF, all three axes are distinct from each other (asymmetric top), as

are the 1D potential profiles of the 5D intermolecular PES along them. Hence, the endohedral PES of H₂@ATOCF exhibits the strongest radial anisotropy, while that of H₂@C₆₀ is the weakest. Another reason for focusing on H₂@ATOCF is that it was the subject of a recent inelastic neutron scattering (INS) investigation,²⁴ in which a number of transitions among the discrete translational and rotational eigenstates of the caged H₂ were observed, providing an opportunity for a direct comparison with theory. The quantum dynamics of H₂ inside ATOCF has been also studied by NMR.^{9,10} The calculations presented here show that, due to the lack of any symmetry on the part of the ATOCF cage, the T-R energy level structure, the quantum numbers required to assign the translational excitations, and the splitting patterns of the rotational excitations, are all completely unlike those encountered for H₂ in C₆₀ (refs 20 and 21) or C₇₀ (ref 23). Extensive comparison is made between the T-R excitations calculated for H₂@ATOCF in the present work and the INS measurements,²⁴ and very good overall agreement is found.

II. Theoretical Methodology

A. Calculations of the Coupled T-R Eigenstates of H₂@ATOCF. The theoretical approach employed in this work is the same as in our studies of H₂@C₆₀ (refs 20 and 21) and H₂@C₇₀ (ref 23). The underlying quantum 5D computational methodology was developed by us earlier for the calculation of the T-R eigenstates of H₂ and its isotopologues inside the cages of the clathrate hydrates.^{16,17,19} The ATOCF cage is treated as rigid, and the geometry determined by the X-ray crystallography²⁵ is used in our calculations. The bond length is held fixed as well. The set of five coordinates (x, y, z, θ , ϕ) is employed; x, y, and z are the Cartesian coordinates of the com of H₂, whereas the two polar angles θ and ϕ specify the orientation of H₂ relative to the cage. The coordinate system is aligned with the three principal axes of ATOCF, and its origin is at the com of the cage. In fact, the principal axes shown in Figure 1 are those determined for the cage without the pyridine and the two phenyl rings attached to the rim of the cage. These three rings hardly interact with the endohedral H₂ and have virtually no influence on its T-R dynamics. However, their masses affect the orientation of the principal axes which, as shown below, is important for a meaningful assignment of the translational excitations. Inspection of the wave function plots discussed later confirms that the translational excitations to a large extent do follow these axes, which greatly simplifies their assignment.

ATOCF is a heavy molecule, its mass equal to 1067 amu, which justifies treating it as nonrotating. Then the 5D T-R Hamiltonian of the caged diatomic molecule is

$$H = -\frac{\mathbf{p}^2}{2\mu} \left(\frac{\partial^2}{\partial x^2} + \frac{\partial^2}{\partial y^2} + \frac{\partial^2}{\partial z^2} \right) + B\mathbf{j}^2 + V(x, y, z, \theta, \phi) \quad (1)$$

where μ is the reduced mass of H₂@ATOCF (2.0122 amu), and \mathbf{j}^2 is the angular momentum operator of the diatomic. The mass of H₂ (2.0160 amu) could have been used instead of μ , since the difference between them is negligible for our purposes. B denotes the rotational constant of the endohedral molecule, and the value of B_{H_2} (59.322 cm⁻¹) was used in our calculations. $V(x, y, z, \theta, \phi)$ in eq 1 is the 5D PES described below. The energy levels and wave functions of the T-R Hamiltonian in eq 1 are obtained with the help of the efficient computational scheme developed in our group.^{16,26} Following a drastic reduc-

tion in size utilizing the sequential diagonalization and truncation procedure,²⁷ the final Hamiltonian matrix is diagonalized yielding the T-R eigenstates which are numerically exact for the 5D PES employed.

In the present calculations, the dimension of the sine-discrete variable representation (DVR) basis was 20 for each of the three Cartesian coordinates x, y, and z, spanning the range -3.78 e

e 3.78 bohr (-3.78, x, y, z). The angular basis included the even-j functions up to j_{\max} 6 for p-H₂ and the odd-j functions up to j_{\max} 7 for o-H₂. The number cutoff parameter for the intermediate 3D eigenvector basis was set to 300, resulting in the final 5D Hamiltonian matrix of dimension 8400 for p-H₂ and 12 800 for o-H₂, respectively. Their diagonalization involved only a modest computational effort, 280 min for p-H₂ and 460 min for o-H₂, on a single processor of a high-performance machine (SGI Altix system).

B. Potential Energy Surface. As in our previous theoretical studies of H₂ in C₆₀ and C₇₀, the 5D interaction potential $V_{H_2-ATOCF}$ between the encapsulated H₂ molecule and $N = 99$ atoms of ATOCF is assumed to be pairwise additive:

$$V_{H_2-ATOCF}(\mathbf{q}) = \sum_{k=1}^N V_{H_2-X}(\mathbf{q}, \mathbf{r}_k) \quad (2)$$

where \mathbf{q} are the coordinates (x, y, z, θ , ϕ) of the endohedral H₂ molecule defined above, V_{H_2-X} is the pair interaction specified below between H₂ and atom X of the fullerene (X = C, N, O, S, H), and the index k runs over all fullerene atoms, whose coordinates \mathbf{r}_k are fixed. There are 80 carbon atoms in ATOCF, of which 63 form the cage and 17 are in the three rings attached to the cage rim. The interactions of H₂ with the carbon atoms are described with the new three-site H₂-C pair potential spectroscopically optimized for H₂@C₆₀ (ref 23) mentioned in the Introduction, denoted $V_{H_2-C, 3s}$:

$$V_{H_2-C, 3s}(\mathbf{q}, \mathbf{r}_k) = V_{LJ}(r_1) + V_{LJ}(r_2) + wV_{LJ}(r_m) \quad (3)$$

In eq 3, V_{LJ} is the standard Lennard-Jones (LJ) 12-6 potential, r_1 and r_2 are the distances of the two H atoms of H₂ from the k th C atom of the fullerene, while r_m is the distance between the midpoint of the H-H bond and the k th C atom. The weight w associated with this third interaction site on H₂ effectively controls the angular anisotropy of the H₂-fullerene interaction PES and allows it to be tuned to the degree that cannot be achieved with the standard two-site H₂-C pair potential.²³ The values of the three parameters of $V_{H_2-C, 3s}$, w , and the weight w , are given in Table 1.

Unlike C₆₀ and C₇₀, ATOCF also has 19 noncarbon atoms, 1 N, 2 O, 1 S, and 14 H atoms, collectively labeled here as Y. Of these, 1 N and 1 S atom belong to the 13-membered orifice, and the 2 O atoms are close to the cage opening. The other noncarbon atoms, 1 N and all 14 H atoms, are situated on the 3 rings, pyridine and 2 phenyl, which, as shown later, have a negligible influence on the T-R dynamics of the H₂ molecule trapped in the fullerene. Even if one were to focus just on the four noncarbon atoms at or near the cage orifice, the amount of pertinent spectroscopic information available is much smaller than what would be needed to optimize the H₂-N/O/S pair potentials along the lines of what was done for the H₂-C pair interaction.²³ Alternatively, these pair potentials could be in principle optimized through ab initio electronic structure calculations involving H₂ and at least a representative fragment

TABLE 1: Parameters Specifying the PESs Used in This Work^a

parameter	Our work (ref 23)	CHARMM	UFF	DREIDING
(H - C)	2.99			
(H - C)	2.95			
w	7.5			
(H - N)		33.55	19.27	12.00
(H - N)		1.283	2.895	3.047
(H - O)		25.99	17.97	13.34
(H - O)		1.236	2.831	2.938
(H - S)		50.32	38.40	25.29
(H - S)		1.329	3.040	3.197
(H - H)		16.09	15.39	5.316
(H - H)		0.400	2.571	2.846

^a (in cm⁻¹) and (in Å) are the LJ parameters and w, defined in the text for the H₂-C interaction only, is dimensionless. The spectroscopically optimized LJ parameters for the H-C pair interaction, and the parameter w, are from our earlier work (ref 23). The columns labeled CHARMM, UFF, and DREIDING give the LJ parameters for the H-X pair interactions (X = N, O, S, H) taken from the CHARMM (CHARMM22) (ref 28), UFF (ref 29), and DREIDING (ref 30) force fields, respectively. For additional explanation see the text.

of ATOCF, at a level sufficiently high to yield reliable energies for the dispersion-dominated H₂-fullerene interactions. Such calculations would be very time-consuming, and although we are likely to take this approach in the future, in the present exploratory study we resort to a much simpler scheme outlined in the following.

For the H₂-Y pair interaction (Y = N, O, S, H), we use the common two-site pair potential V_{H₂-Y,2s},

$$V_{\text{H}_2-\text{Y},2s}(\mathbf{q}, \mathbf{r}) \propto V_{\text{LJ}}(r_1) + V_{\text{LJ}}(r_2) \quad (4)$$

where V_{LJ}, r₁, and r₂ have the same meaning as in eq 3. Three different sets of the heteronuclear LJ parameters _{HY} and _{HY} were obtained from the appropriate homonuclear parameters for the nonbonded interactions in the CHARMM (CHARMM22),²⁷ UFF,²⁹ and DREIDING³⁰ force fields, respectively, using the standard geometric-mean combination rules. Their values are listed in Table 1. They allow us to test the sensitivity of the calculated T-R energy levels to the parameters of the H₂-Y pair potentials. We are fully aware of the shortcomings of this approach. It is ad hoc and somewhat inconsistent, since the H₂-noncarbon interactions are described using the LJ parameters taken from the force fields, while the H₂-C pair potential was optimized based on the IR spectroscopy of H₂@C₆₀. On a more subtle level, since the parameters in the force fields were developed for the use in classical simulations, with the aim of reproducing various experimentally measured properties, they already incorporate some quantum effects, such as the intermolecular ZPE among others, to an uncertain degree. Therefore, one can argue that these parameters will not perform optimally when used in the quantum mechanical calculations, where the quantum effects that are treated rigorously come on top of those implicitly present in the force-field parameters. Our response is that this pragmatic approach, its weaknesses notwithstanding, is the only one which presently allows us to rapidly generate a 5D intermolecular PES for H₂@ATOFC. Moreover, the quality of the PES is tested directly and unambiguously by comparing the T-R excitations calculated on it with the experimental data from the INS spectroscopy; the comparison discussed below shows that this PES is capable of providing the T-R energy levels structure which is at least semiquantitatively accurate.

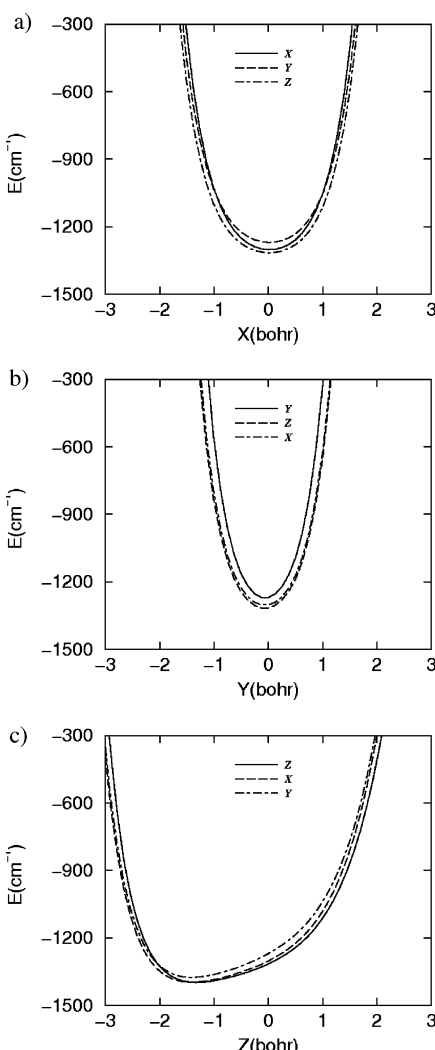


Figure 2. One-dimensional cuts through the 5D PES of H₂@ATOFC, constructed using the spectroscopically optimized (ref 23) LJ parameters for the H-C pair interaction, and the parameter w, and the CHARMM LJ parameters for the H-Y pair interactions (Y = N, O, S, H), all given in Table 1. Three potential curves are shown for each 1D cut, one for H₂ parallel to the axis of motion (full line), and the other two for H₂ parallel to either of the two axes perpendicular to the axis of motion: (a) along the x axis, (b) along the y axis, (c) along the z axis.

The 1D profiles of the 5D PES of H₂@ATOFC, generated using the spectroscopically optimized three-site H₂-C pair potential and the CHARMM parameters for the H₂-Y (Y = N, O, S, H) pair interactions, along the x, y, and z axes are displayed in Figure 2. The x, y, and z coordinates of the global minimum of the PES are (in bohr) (0.06, -0.02, -1.32), that is, the z coordinate of the global minimum, unlike its x and y coordinates, does not coincide with that of the com of ATOCF, which defines the origin of the Cartesian coordinate system. For this reason, the minimum of the 1D profile along the z axis in Figure 2c is not at z = 0. The three 1D cuts differ considerably, with the one along z being the most anharmonic, which is evidence of the strong anisotropy of the 5D PES with respect to the directions in which the com of H₂ moves away from the center of the cage. This reflects in the quantum T-R dynamics discussed in the following section.

III. Results and Discussion

The T-R energy levels from the quantum 5D calculations on the pairwise additive PES described in the preceding section,

TABLE 2: T-R Energy Levels of *p*-H₂ Molecule in ATOCF^a

<i>i</i>	ΔE	Δx	Δy	Δz	(V _x , V _y , V _z)	<i>j</i> ⊥ 0	<i>j</i> ⊥ 2
0	0.00	0.44	0.36	0.50	(0, 0, 0)	1.00	0.00
1	118.31	0.42	0.35	0.84	(0, 0, 1)	1.00	0.00
2	149.48	0.73	0.36	0.47	(1, 0, 0)	1.00	0.00
3	230.93	0.43	0.59	0.47	(0, 1, 0)	1.00	0.00
4	242.04	0.42	0.34	1.05	(0, 0, 2)	1.00	0.00
5	282.69	0.70	0.35	0.80	(1, 0, 1)	0.99	0.01
6	322.46	0.88	0.37	0.47	(2, 0, 0)	0.99	0.01
7	349.13	0.44	0.37	0.50	(0, 0, 0)	0.00	1.00
8	349.14	0.45	0.37	0.50	(0, 0, 0)	0.01	0.99
9	356.90	0.44	0.40	0.56	(0, 0, 0)	0.15	0.85
10	360.34	0.45	0.37	0.50	(0, 0, 0)	0.02	0.98
11	363.95	0.45	0.36	0.50	(0, 0, 0)	0.01	0.99
12	367.92	0.42	0.55	0.76	(0, 1, 1)	0.85	0.15
13	374.63	0.41	0.34	1.20	(0, 0, 3)	0.99	0.01
14	396.64	0.70	0.58	0.45	(1, 1, 0)	0.98	0.02
15	420.65	0.69	0.34	1.00	(1, 0, 2)	0.98	0.02
16	464.64	0.61	0.35	0.83	(0, 0, 1)	0.34	0.66
17	467.19	0.43	0.35	0.84	(0, 0, 1)	0.01	0.99
18	470.33	0.73	0.35	0.80	(2, 0, 1)	0.63	0.37
19	476.25	0.43	0.36	0.85	(0, 0, 1)	0.03	0.97
20	479.23	0.43	0.35	0.84	(0, 0, 1)	0.01	0.99
21	483.13	0.43	0.35	0.84	(0, 0, 1)	0.01	0.99
22	492.34	0.42	0.72	0.46	(0, 2, 0)	0.99	0.01
23	497.03	0.75	0.37	0.47	(1, 0, 0)	0.06	0.94
24	500.02	0.73	0.37	0.49	(1, 0, 0)	0.03	0.97
25	505.18	0.61	0.46	0.78	(?, ?, ?)	0.44	0.56
26	505.25	0.58	0.48	0.82	(?, ?, ?)	0.53	0.47
27	511.85	0.73	0.37	0.47	(1, 0, 0)	0.02	0.98
28	512.16	0.80	0.36	0.47	(1, 0, 0)	0.21	0.79
29	516.85	0.42	0.34	1.31	(0, 0, 4)	0.99	0.01
30	518.82	0.92	0.37	0.47	(3, 0, 0)	0.71	0.29
...
33	573.90	0.49	0.60	0.47	(0, 1, 0)	0.10	0.90
34	575.39	0.43	0.60	0.47	(0, 1, 0)	0.01	0.99
35	584.23	0.82	0.58	0.44	(2, 1, 0)	0.88	0.12
36	589.82	0.42	0.37	1.03	(0, 0, 2)	0.01	0.99
37	591.85	0.44	0.36	1.04	(0, 0, 2)	0.06	0.94
38	592.54	0.43	0.58	0.55	(0, 1, 0)	0.01	0.99
39	595.19	0.43	0.58	0.53	(0, 1, 0)	0.01	0.99
40	600.21	0.42	0.39	1.01	(0, 0, 2)	0.02	0.98
41	602.24	0.43	0.56	0.61	(0, 1, 0)	0.01	0.99
42	603.26	0.42	0.34	1.05	(0, 0, 2)	0.00	1.00
43	607.42	0.42	0.34	1.05	(0, 0, 2)	0.01	0.99
44	616.80	0.81	0.36	0.96	(2, 0, 2)	0.81	0.19
...
60	695.00	0.65	0.56	0.95	(1, 1, 2)	0.87	0.13
65	728.24	1.01	0.41	0.51	(4, 0, 0)	0.85	0.15
82	779.91	0.42	0.82	0.45	(0, 3, 0)	0.98	0.02
88	801.69	0.40	0.56	1.27	(0, 1, 4)	0.97	0.03
92	828.74	0.42	0.37	1.45	(0, 0, 6)	0.94	0.06

^a The excitation energies ΔE (in cm⁻¹) are relative to the ground-state energy E_0 = -1167.068 cm⁻¹. Also shown are the rms amplitudes Δx , Δy , and Δz (in bohr), and the Cartesian quantum number assignments (V_x, V_y, V_z). The columns labeled *j* ⊥ 0 and *j* ⊥ 2 show the contributions from these rotational basis functions to the wave functions. The numbers in boldface are used for the states that are predominantly *j* ⊥ 2.

in which the CHARMM²⁸ LJ parameters in Table 1 are used for the H₂–Y pair interactions (Y = N, O, S, H) in combination with the three-site H₂–C pair potential (Table 1), are shown for *p*-H₂@ATOCF in Table 2 and for *o*-H₂@ATOCF in Table 3. For each state, the root-mean-square (rms) amplitudes Δx , Δy , and Δz are given, which measure the wave function delocalization along the respective Cartesian coordinates and are helpful in making the quantum number assignments. Listed next to the rms amplitudes are the translational quantum number assignments discussed below. Finally, the columns labeled *j* ⊥ 0 and *j* ⊥ 2 in Table 2, and *j* ⊥ 1 and *j* ⊥ 3 in Table 3, show the contributions of these rotational basis functions to the eigenstates of the encapsulated *p*-H₂ and *o*-H₂, respectively. They

were determined by projecting the T-R wave functions on the rotational basis, taking the moduli squared and integrating over *x*, *y*, and *z* coordinates. The global minimum of the PES lies at -1398.258 cm⁻¹, and the T-R ground-state energy E_0 is -1167.068 cm⁻¹. Therefore, the ZPE associated with the T-R modes is 231.190 cm⁻¹, or 16.5% of the potential well depth; this is close to the ZPE of 241.55 cm⁻¹ calculated for H₂@C₆₀ and is considerably greater than the ZPE calculated for H₂@C₇₀, 145.74 cm⁻¹ (ref 23).

A. Translational Excitations. A glance at the T-R energy levels of H₂@ATOCF displayed in Tables 2 and 3 shows that they do not exhibit any pattern of degeneracies, in contrast to those of H₂@C₆₀ (refs 20 and 21) and H₂@C₇₀ (ref 23), where

TABLE 3: T-R Energy Levels of *o*-H₂ Molecule in ATOCF^a

<i>i</i>	ΔE	Δx	Δy	Δz	(V _x , V _y , V _z)	$j \rightarrow 1$	$j \rightarrow 3$
1	112.01	0.45	0.36	0.50	(0, 0, 0)	1.00	0.00
2	115.41	0.44	0.36	0.50	(0, 0, 0)	1.00	0.00
3	129.06	0.45	0.36	0.50	(0, 0, 0)	1.00	0.00
4	229.80	117.79	0.43	0.35	0.84 (0, 0, 1)	1.00	0.00
5	233.02	117.61	0.42	0.35	0.84 (0, 0, 1)	1.00	0.00
6	248.44	119.39	0.43	0.34	0.84 (0, 0, 1)	1.00	0.00
7	259.12	147.11	0.73	0.37	0.47 (1, 0, 0)	1.00	0.00
8	268.35	152.94	0.72	0.37	0.47 (1, 0, 0)	1.00	0.00
9	277.66	148.60	0.73	0.36	0.47 (1, 0, 0)	1.00	0.00
10	339.41	227.40	0.43	0.60	0.47 (0, 1, 0)	1.00	0.00
11	343.18	227.47	0.43	0.60	0.47 (0, 1, 0)	1.00	0.00
12	353.36	241.35	0.43	0.35	1.05 (0, 0, 2)	1.00	0.00
13	356.47	241.06	0.42	0.34	1.05 (0, 0, 2)	1.00	0.00
14	368.84	239.78	0.43	0.58	0.48 (0, 1, 0)	1.00	0.00
15	372.75	243.69	0.42	0.34	1.05 (0, 0, 2)	1.00	0.00
...
57	703.76	0.44	0.37	0.50	(0, 0, 0)	0.00	1.00
58	703.77	0.44	0.37	0.50	(0, 0, 0)	0.00	1.00
59	711.87	0.45	0.36	0.50	(0, 0, 0)	0.00	1.00
60	712.15	0.44	0.36	0.50	(0, 0, 0)	0.00	1.00
61	716.68	0.45	0.36	0.50	(0, 0, 0)	0.00	1.00
63	718.86	0.44	0.36	0.50	(0, 0, 0)	0.00	1.00
64	720.86	0.44	0.36	0.50	(0, 0, 0)	0.00	1.00
...
85	821.36	117.61	0.43	0.35	0.85 (0, 0, 1)	0.01	0.99
86	821.44	117.68	0.43	0.35	0.84 (0, 0, 1)	0.00	1.00
88	830.38	118.51	0.43	0.35	0.84 (0, 0, 1)	0.00	1.00
89	830.51	118.35	0.43	0.35	0.84 (0, 0, 1)	0.01	0.99
91	835.73	119.05	0.45	0.36	0.85 (0, 0, 1)	0.06	0.94
93	838.09	119.22	0.47	0.38	0.87 (0, 0, 1)	0.14	0.86
94	839.66	119.53	0.44	0.36	0.84 (0, 0, 1)	0.04	0.96
...
99	853.78	150.03	0.73	0.37	0.47 (1, 0, 0)	0.00	1.00
100	853.95	150.19	0.73	0.37	0.48 (1, 0, 0)	0.00	1.00
102	860.05	148.18	0.74	0.38	0.49 (1, 0, 0)	0.06	0.94
104	861.98	149.82	0.73	0.37	0.48 (1, 0, 0)	0.01	0.99
105	864.31	147.63	0.73	0.36	0.47 (1, 0, 0)	0.00	1.00
106	870.57	151.70	0.72	0.36	0.47 (1, 0, 0)	0.01	0.99
107	870.96	150.83	0.73	0.36	0.47 (1, 0, 0)	0.01	0.99
...
121	928.87	225.11	0.43	0.60	0.47 (0, 1, 0)	0.00	1.00
122	928.87	225.10	0.43	0.60	0.47 (0, 1, 0)	0.00	1.00
129	943.62	231.75	0.45	0.56	0.78 (0, 1, 0)?	0.19	0.81
130	943.90	231.74	0.45	0.54	0.87 (0, 1, 0)?	0.24	0.76
135	953.64	236.96	0.43	0.52	0.78 (0, 1, 0)?	0.03	0.97
138	956.40	237.54	0.43	0.57	0.58 (0, 1, 0)	0.03	0.97
144	962.64	242.52	0.43	0.60	0.58 (0, 1, 0)	0.16	0.84

^a The excitation energies ΔE are measured from the T-R ground-state energy $E_0 \rightarrow -1167.068 \text{ cm}^{-1}$ of the caged *p*-H₂. Other symbols have the same meaning as in Table 2. The energies in the third column for the $j \rightarrow 1$ states are relative to those of the states $i \rightarrow 1-3$, whereas for the $j \rightarrow 3$ states they are relative to the states $i \rightarrow 57-61, 63, 64$. The numbers in boldface are used to highlight the septets of $j \rightarrow 3$ levels corresponding to the translational ground state and the fundamental excitations of the *x*, *y*, and *z* modes, and also for the three $j \rightarrow 1$ levels in the ground translational state ($i \rightarrow 1-3$). For additional explanation see the text. All energies are in cm^{-1} .

the degeneracies are pervasive. This qualitative difference in the T-R energy level structure signals that neither of the sets of quantum numbers used to assign the translationally excited states of H₂ in C₆₀ or C₇₀ is applicable to H₂@ATOFC. What quantum numbers are appropriate for H₂@ATOFC becomes clear upon inspection of Figures 3–6, which for the translationally excited ($j \neq 0$) T-R eigenstates in Table 2 show the 3D reduced probability density (RPD) $F_i(x, y, z)$ in the translational (Cartesian) coordinates¹⁶

$$F_i(x, y, z) \propto \int |\psi_i(x, y, z, \dots)|^2 |F_i(x, y, z, \dots)|^2 dxdydz \quad (5)$$

where $\psi_i(x, y, z, \dots)$ is the *i*th T-R eigenfunction of the encapsulated *p*-H₂ or *o*-H₂. The RPDs in Figures 3–5 reveal

the existence of well-defined quasi-1D translational modes along the *x*, *y*, and *z* axes. The strikingly regular nodal patterns of their excitations allow a straightforward assignment in terms of the Cartesian quantum numbers V_x, V_y, or V_z, by counting the number of nodal planes perpendicular to the *x*, *y*, or *z* axis, respectively. The utility of the Cartesian quantum numbers is not limited to the single-mode excitations (V_x, 0, 0), (0, V_y, 0), and (0, 0, V_z). As Figure 6 shows, the combination states where two or all three translational modes are excited also have rather regular wave functions and are readily assignable using the triplets of Cartesian quantum numbers (V_x, V_y, V_z). This is true for the large majority, although not all, of the T-R states in Tables 2 and 3.

That the Cartesian quantum numbers are appropriate for the assignment of the excited T-R states of H₂@ATOFC is easily

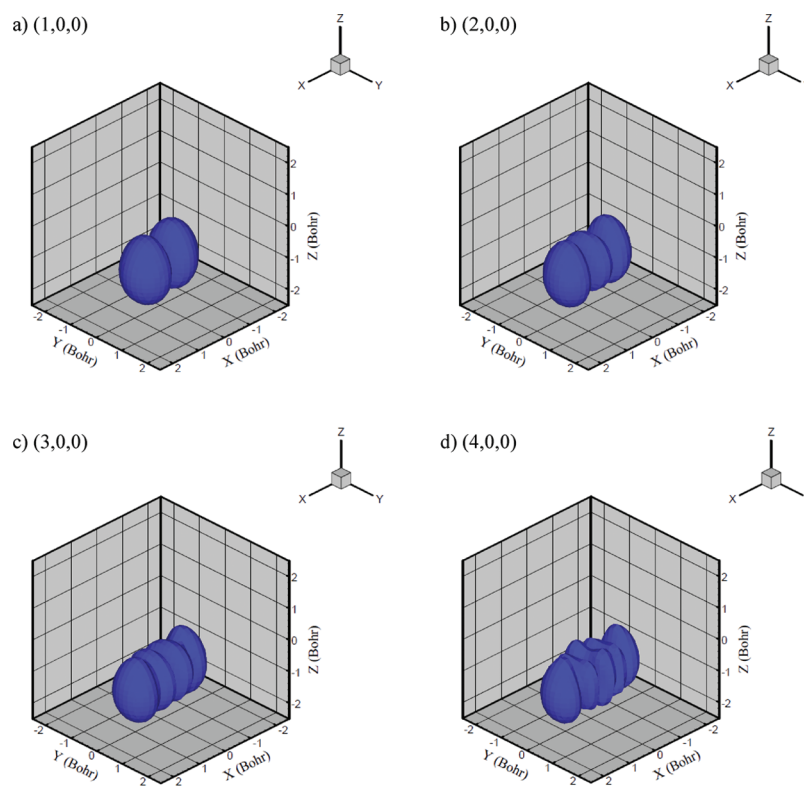


Figure 3. 3D isosurfaces of the reduced probability density in the translational (Cartesian) coordinates of the $j \geq 0$ T-R states ($V_x, 0, 0$), $V_x = 1 - 4$, of $p\text{-H}_2@\text{ATOCF}$, listed in Table 2. The x axis is shown in Figure 1. The isosurfaces are drawn at 10% of the maximum value of the density.

understood, and actually anticipated, in view of the fact mentioned earlier that the profiles of the 5D PES along the three principal axes of ATOCF, shown in Figure 2, are very different. Also different are the frequencies of the x -mode fundamental ($1, 0, 0$), 149.5 cm^{-1} , the y -mode fundamental ($0, 1, 0$), 230.9 cm^{-1} , and the z -mode fundamental ($0, 0, 1$), 118.3 cm^{-1} . The z mode, which is directed toward the cage orifice, has the lowest frequency, consistent with the relatively soft and anharmonic potential profile along the z axis shown in Figure 2c. The fundamental frequency of the y mode is much higher than that of the other transverse (x) mode, a consequence of the considerably greater stiffness of the PES (and narrower cage) in the y direction than in the x direction [Figures 2a,b]. Thus, the absence of symmetry in the ATOCF cage leads to complete splitting of the translational fundamental in three distinct excitations, along each of the principal axes of the cage. For comparison, in the most highly symmetric fullerene C_{60} , the translational fundamental is triply degenerate,^{20,23} whereas in C_{70} , in which two axes (x and y) are equivalent and the third (z) is distinct, the translational fundamental splits into a doubly degenerate xy pair and a nondegenerate z excitation.²³

A closer inspection of Table 2 reveals that all three translational modes exhibit substantial negative anharmonicity, that is, the energy differences between the successive members of a pure mode progression increase with the number of quanta in that mode. For example, in the x -mode progression ($V_x, 0, 0$), where the energy of the fundamental ($1, 0, 0$) is 149.5 cm^{-1} , the energy difference between ($1, 0, 0$) and ($2, 0, 0$) is 173.0 cm^{-1} , increasing to 196.4 cm^{-1} between ($2, 0, 0$) and ($3, 0, 0$), and to 209.4 cm^{-1} between ($3, 0, 0$) and ($4, 0, 0$). In the y -mode progression ($0, V_y, 0$), with the fundamental ($0, 1, 0$) at 230.9 cm^{-1} , the next member ($0, 2, 0$) lies 261.4 cm^{-1} higher, whereas ($0, 3, 0$) is 287.6 cm^{-1} above ($0, 2, 0$). The same holds for the progression ($0, 0, V_z$) in the z mode. Its fundamental ($0, 0, 1$)

has the energy of 118.3 cm^{-1} ; the energy separation between the neighboring levels increases steadily with V_z , reaching 160.3 cm^{-1} between ($0, 0, 5$) and ($0, 0, 6$). Negative anharmonicity is also displayed by the translational excitations which we have calculated for $\text{H}_2@\text{C}_{60}$ (refs.²⁰ and²³) and $\text{H}_2@\text{C}_{70}$ (ref.²³).

The rms amplitudes Δx , Δy , and Δz grow rapidly with the excitation of the x , y , and z modes, respectively. The extent of delocalization is the largest in the case of the z mode, aimed at the opening in the cage; Δz is 0.84 au for ($0, 0, 1$), it increases to 1.05 au for ($0, 0, 2$), and it reaches 1.45 au for ($0, 0, 6$). This is to be expected, since Figure 2 shows the potential profile in the z direction to be significantly more open than along the x and y axes, allowing for larger amplitudes of motion in this direction.

The wave functions of most of the T-R states considered appear to have regular nodal patterns implying weak to moderate coupling among the translational modes. One measure of the degree of mode coupling is the deviation of the energy of the combination state from the sum of the relevant excitations of the pure modes. Thus, the energy of the state ($1, 0, 1$) in Table 2, 282.7 cm^{-1} , is 14.9 cm^{-1} higher than the sum of the energies of ($1, 0, 0$) and ($0, 0, 1$), 149.5 and 118.3 cm^{-1} , which is 267.8 cm^{-1} . For the state ($2, 0, 1$), its energy of 470.3 cm^{-1} is 29.5 cm^{-1} larger than the sum of the energies of the states ($2, 0, 0$) and ($0, 0, 1$), 440.8 cm^{-1} . States involving combined excitations of other translational modes show similar behavior.

B. Rotational Excitations and T-R Coupling. So far, our discussion has dealt only with the translational excitations of H_2 (in the ground translational state $j \geq 0$) inside ATOCF. We now turn our attention to the rotationally excited states of the encapsulated H_2 and the issue of T-R coupling. First we address the question of how good a quantum number j actually is. Our previous studies of H_2 in C_{60} (refs 20, 21, and 23) and C_{70} (ref 23) found that apart from a couple of nearly degenerate states,

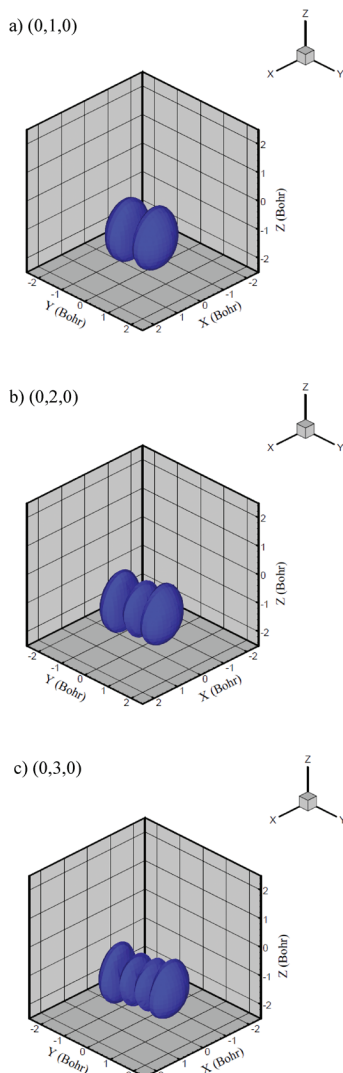


Figure 4. 3D isosurfaces of the reduced probability density in the translational (Cartesian) coordinates of the $j \geq 0$ T-R states $(0, V_y, 0)$, $V_y \geq 1 - 3$, of $p\text{-H}_2$ @ATOFC, listed in Table 2. The y axis is shown in Figure 1. The isosurfaces are drawn at 10% of the maximum value of the density.

j is a good quantum number in these two endohedral complexes, in the range of the excitation energies considered. In the case of H₂@ATOFC, for the large majority of T-R states of $p\text{-H}_2$ and $o\text{-H}_2$ shown in Tables 2 and 3, respectively, j is a good quantum number as well, since the contribution of the dominant rotational basis function, $j \geq 0$ or 2 for $p\text{-H}_2$ and $j \geq 1$ or 3 for $o\text{-H}_2$, is typically greater than 0.8, and in fact greater than 0.9 in most cases. Apparently, the large anisotropy of the ATOCF cage does not induce significant mixing of the rotational basis function with different j values. However, a few states do show strong j mixing, such as those of $p\text{-H}_2$, $i \geq 25$ (44% $j \geq 0$, 56% $j \geq 2$) and $i \geq 26$ (53% $j \geq 0$, 47% $j \geq 2$) which are very close in energy, and to a somewhat lesser degree, $i \geq 16$ and $i \geq 18$.

From Table 3 one can see that the 3-fold degeneracy of the $j \geq 1$ level of $o\text{-H}_2$ is completely lifted by the angular anisotropy of the PES, and the splitting of the $j \geq 1$ triplet in the ground translational state $(0, 0, 0)$ is 17.1 cm^{-1} . The $j \geq 3$ level of $o\text{-H}_2$, which is 7-fold degenerate in the gas phase, is split into a pair of almost degenerate states and five nondegenerate states of higher energies. Interestingly, their spread over 17.1 cm^{-1} in the ground translational state $(0, 0, 0)$ is identical to that of the

$j \geq 1$ triplet. The 5-fold degeneracy of the $j \geq 2$ level of the gas-phase $p\text{-H}_2$ in the ATOCF is split into a nearly degenerate pair and three nondegenerate higher-energy states, as shown in Table 2. In the ground translational state $(0, 0, 0)$, these five states are split by 14.8 cm^{-1} . The presence of an almost degenerate pair of states in the splitting patterns both $j \geq 2$ and $j \geq 3$ multiplets is curious, since it is not required by symmetry or group-theoretical arguments, as ATOCF has no symmetry. In C₆₀, the $(2j + 1)$ -fold degeneracy of the $j \geq 1 - 3$ levels of H₂ is completely preserved, apart from a tiny 4:3 splitting of the $j \geq 3$ septet induced by the icosahedral I_h environment of C₆₀.²⁰ Inside C₇₀, the $j \geq 1$ triplet of $o\text{-H}_2$ is split into a single state and a pair of degenerate states, whereas the $j \geq 2$ quintuplet of $p\text{-H}_2$ is split in a 1:2:2 degeneracy pattern. Both splitting patterns can be explained in terms of the group theory.²³

Fundamental excitation of the two lower-frequency x and z modes causes only small changes in the magnitude of the splittings of the $j \geq 1 - 3$ multiplets. Thus, the $j \geq 1$ triplet is split by 18.6 and 18.5 cm^{-1} in the states $(0, 0, 1)$ and $(1, 0, 0)$, respectively, compared to 17.1 cm^{-1} for $(0, 0, 0)$. For $j \geq 3$, the quintuplet splitting is 18.3 and 17.2 cm^{-1} for $(0, 0, 1)$ and $(1, 0, 0)$, respectively, relative to 17.1 cm^{-1} in the state $(0, 0, 0)$. However, exciting the highest-frequency y mode leads to a significant increase in the splitting of the rotational multiplets. In the state $(0, 1, 0)$, the splitting of the $j \geq 1$ triplet is 29.4 cm^{-1} , and 33.8 cm^{-1} for the $j \geq 3$ septet. The $j \geq 2$ quintuplet exhibits very similar trends.

Finally, we briefly discuss the translational excitations of $o\text{-H}_2$ in the $j \geq 1$ and $j \geq 3$ states (Table 3), and compare them with the translational excitations of $p\text{-H}_2$ (Table 2). In the third column of Table 3, the energies of the triplets, for $j \geq 1$, or the septets for $j \geq 3$ having the same translational quantum numbers represent the difference between their excitation energies (ΔE) in the second column and the excitation energies of the corresponding $j \geq 1$ or $j \geq 3$ multiplets in the ground translational state $(0, 0, 0)$. Hence, they represent the purely translational excitation energies out of different sublevels of $j \geq 1$ and $j \geq 3$, respectively, in the state $(0, 0, 0)$. We focus on the translational fundamentals originating from the $j \geq 1$ triplet for $(0, 0, 0)$. One finds that their energy spread is 1.6 cm^{-1} for $(0, 0, 1)$, 5.8 cm^{-1} for $(1, 0, 0)$, and 12.4 cm^{-1} for $(0, 1, 0)$. The $(0, 0, 1)$ excitation energies lie within $\pm 1 \text{ cm}^{-1}$, on both low- and high-energy side, of the corresponding $j \geq 0$ fundamental and within $\pm 3 \text{ cm}^{-1}$ of the $j \geq 0$ value for $(1, 0, 0)$. In the case of the $(0, 1, 0)$ fundamental, its three $j \geq 1$ components are at 227.4 , 227.5 , and 239.8 cm^{-1} , compared to 230.9 cm^{-1} for $j \geq 0$.

C. Comparison between Theory and INS Spectroscopy. The INS spectrum of H₂@ATOFC reported by Horsewill and co-workers²⁴ shows five peaks whose energies are given in Table 4. The three lower-energy peaks at 106.9 , 119.0 , and 129.9 cm^{-1} , were assigned to the $j \geq 0$ f $j \geq 1$ rotational transition. The two peaks at higher energies, 137.9 and 144.4 cm^{-1} , were attributed to two translational fundamentals, out of the three expected for the anisotropic cage of ATOCF.²⁴ Table 4 also gives the corresponding theoretical values from our quantum 5D calculations. Actually, three sets of theoretical results are shown, obtained for three LJ parameter sets for the H-Y pair interactions (Y = N, O, S, H) designated as CHARMM, UFF, and DREIDING, which are listed in Table 1. The spectroscopically optimized three-site H₂-C pair potential (Table 1) is used in all the calculations.

Theory and the INS measurements are in agreement that the anisotropy of the ATOCF cage causes complete removal of the

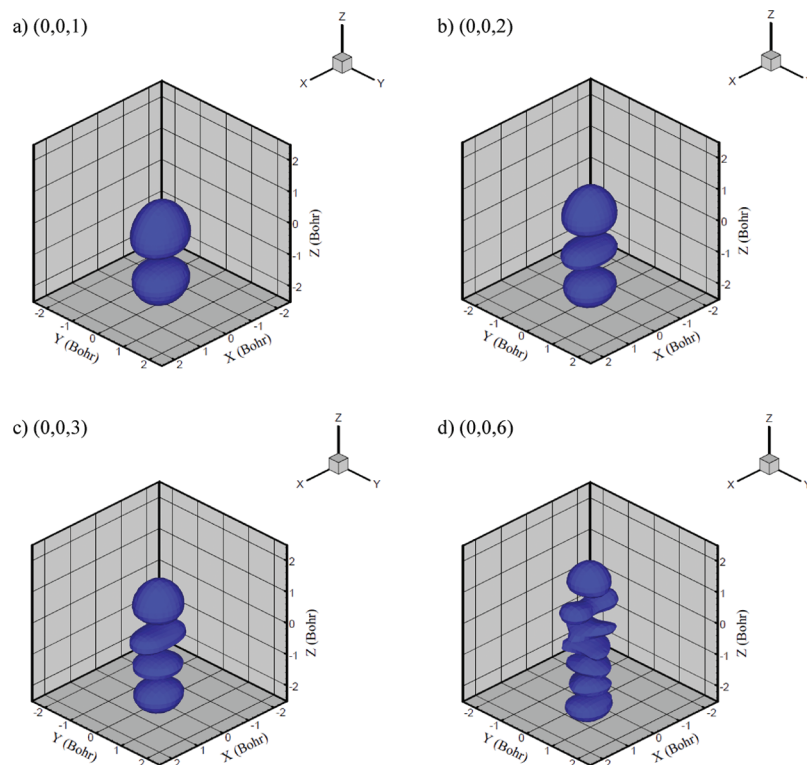


Figure 5. 3D isosurfaces of the reduced probability density in the translational (Cartesian) coordinates of the $j \rightarrow 0$ T-R states $(0, 0, V_z)$, $V_z = 1 - 3, 6$, of $p\text{-H}_2$ @ATOCF, listed in Table 2. The z axis is shown in Figure 1. The isosurfaces are drawn at 10% of the maximum value of the density.

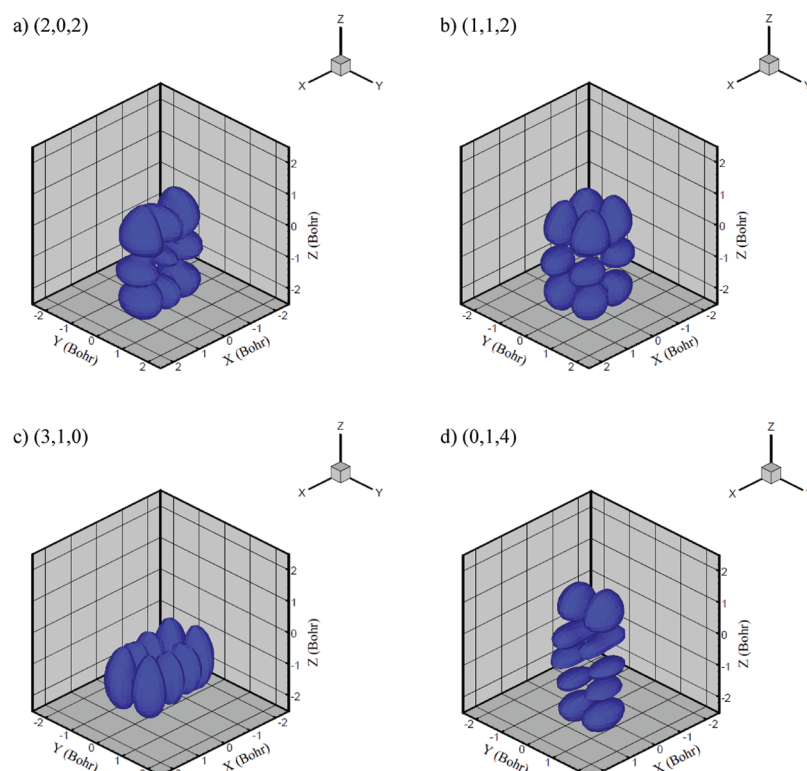


Figure 6. 3D isosurfaces of the reduced probability density in the translational (Cartesian) coordinates of four $j \rightarrow 0$ T-R combination states of $p\text{-H}_2$ @ATOCF, where two or all three translational modes are excited, listed in Table 2. The isosurfaces are drawn at 10% of the maximum value of the density.

three-fold degeneracy of the $j \rightarrow 1$ rotational level of the encapsulated $\sigma\text{-H}_2$ molecule, so that the $j \rightarrow 0 \leftarrow j \rightarrow 1$ transition is split into a triplet. The calculated and observed components of the $j \rightarrow 1$ triplet lie in the same energy range. The splitting

calculated for the ground translational state $(0, 0, 0)$, 17.1 cm^{-1} , is close to the experimental value of 23.0 cm^{-1} . The fact that the theoretical result is about 25% smaller than the measured one suggests that our PES underestimates somewhat the actual

TABLE 4: Comparison of the $j \rightarrow 0$ f $j \rightarrow 1$ Rotational Transitions and the Fundamental Translational Excitations Calculated in This Work with Those from the INS Spectra in Reference 24^a

	exp.	CHARMM	UFF	DREIDING
$j \rightarrow 0$ f $j \rightarrow 1$				
I	106.9	112.0	(112.1)	111.2
II	119.0	115.4	(115.4)	115.9
III	129.9	129.1	(129.0)	129.4
Δ	23.0	17.1	(16.9)	18.2
translational fundamentals				
z	137.9	118.3	(119.5)	112.8
x	144.4	149.5	(149.5)	149.7
y	230–240 ^b	230.9	(230.9)	231.2
				231.2

^a Δ denotes the splitting of the $j \rightarrow 1$ triplet. The columns labeled CHARMM, UFF, and DREIDING give our results computed on the three PESs for which the LJ parameters of the H-Y pair interactions (Y = N, O, S, H) are listed in Table 1. The numbers in brackets are for the ATOCF cage without the three rings. The spectroscopically optimized LJ parameters for the H-C pair interaction, and the parameter w , also given in Table 1, are used in all three PESs. For additional explanation see the text. All energies are in cm⁻¹. ^b Estimated (ref 24).

angular anisotropy of the interaction potential between H₂ and the interior of the ATOCF cage. We also note that the calculated energies of the components of the $j \rightarrow 1$ triplet are virtually the same for all three sets (CHARMM, UFF, DREIDING) of the LJ parameters of the H-Y pair interactions (Y = N, O, S, H) employed in this study.

The experimentally observed translational peaks are mainly due to the *o*-H₂ molecules.²⁴ Consequently, in order to compare our calculated translational fundamentals with experiment, for each one we could have used the average of the (three) excitation energies originating from the three components of the $j \rightarrow 1$ triplet of *o*-H₂ shown in Table 3, discussed in the preceding section. However, these average values are nearly identical to the corresponding translational fundamentals of ($j \rightarrow 0$) *p*-H₂ in Table 2. Hence for simplicity, the latter are given in Table 4.

The two reported translational peaks clearly correspond to our z - and x -mode fundamentals, respectively. The calculated energy of the x -mode fundamental, 149.5 cm⁻¹, agrees very well with the translational peak observed at 144.4 cm⁻¹. But, the theoretical result for z -mode fundamental, 118.3 cm⁻¹, is 14% smaller than the lowest-energy INS peak at 137.9 cm⁻¹. We believe that the reason why the agreement between theory and experiment for the z -mode excitation is not as good as for the x -mode fundamental is the following. As shown clearly in Figure 7 for the state (0, 0, 6), the z -mode excitations point almost directly toward the orifice of ATOCF where the N and S atoms are situated (and the two O atoms are nearby), and therefore probe the PES in the vicinity of the heteroatoms. This makes the z mode much more sensitive to how well the PES describes the interactions of H₂ with the noncarbon atoms than the x -mode (and y -mode) excitations; the latter interact primarily with the carbon atoms forming the body of the cage. The greater difference between the calculated and measured energies of the z -mode fundamental suggests that the description of the H₂-noncarbon (N, O, S, H) interactions in H₂@ATOFC using the two-site pair potentials with the LJ parameters taken directly from various force field is not as accurate as the description of the H₂-carbon interactions in terms of the three-site H₂-C pair potential. This is not surprising, since the parameters of the three-site H₂-C pair potential have been spectroscopically

optimized (for H₂@C₆₀),²³ which is not the case with the LJ parameters of the H₂-noncarbon pair potentials.

Horsewill and co-workers did not report the experimental value for the third translational fundamental.²⁴ On the basis of the considerations of the geometrical features of ATOCF and scaling the observed translational excitations at 140 cm⁻¹, they estimated that the energy of the third translational peak should be approximately 230–240 cm⁻¹. Our calculated y -mode fundamental at 230.9 cm⁻¹ agrees nicely with their estimate. A band of overlapping peaks was observed in the INS spectra,²⁴ in the range 230–320 cm⁻¹. No assignment was attempted because of the expected presence of other translational excitations and cage deformation modes in this region. Table 2 shows that several calculated excitations besides the y -mode fundamental (0, 1, 0), such as (0, 0, 2), (1, 0, 1), and (2, 0, 0), have energies between 230 and 320 cm⁻¹, making them natural candidates for assigning this region of the INS spectrum.

In closing of this section, we point out that energies of both the $j \rightarrow 1$ triplet and the translational fundamentals calculated for the ATOCF structure from which the pyridine and the two phenyl rings have been removed, given by the numbers in brackets in Table 4, differ negligibly from those for ATOCF with the three rings in place. This demonstrates that these three rings have very little influence on the T-R dynamics of the trapped H₂, at least at relatively low excitation energies.

IV. Conclusions

We have performed fully coupled quantum 5D calculations of the T-R energy levels and wave functions of H₂ encapsulated inside ATOCF, in order to characterize the salient features of the T-R dynamics in a fullerene without any symmetry. This study adds to our understanding of how the symmetry of the nanocage, or lack of it in this case, influences the quantum dynamics of the guest hydrogen molecule, the topic previously explored by us in the investigations of H₂ inside high-symmetry fullerenes, C₆₀ (I_h)^{20,21,23} and C₇₀ (D_{5h}).²³ A pairwise additive 5D intermolecular PES was constructed using the novel three-site H₂-C pair potential spectroscopically optimized for H₂@C₆₀ (ref.²³) for the H₂-carbon interactions, while the interactions between H₂ and the noncarbon atoms of ATOCF (N, O, S, H) were described in terms of the two-site pair potentials whose LJ parameters were taken from three widely used force fields.

The lack of symmetry in ATOCF translates into the PES whose profiles along the three principal axes x , y , and z differ substantially; hence, the radial anisotropy of this PES is much larger than for H₂ in either C₆₀ or C₇₀. The plots of the 3D reduced probability densities (RPDs) revealed three well-defined quasi-1D translational modes, one along each of the principal axes, and that the Cartesian quantum numbers (V_x , V_y , V_z) are appropriate for the assignment of these and other translationally excited eigenstates. The strong anisotropy of the intermolecular PES results in the complete splitting of the translational fundamental into three excitations with very different frequencies; the z mode, which is directed toward the orifice of the cage, has the lowest frequency and is the most anharmonic. For perspective, the translational fundamental of H₂ in C₆₀ is triply degenerate, and that of H₂ in C₇₀ is partially split into a doubly degenerate pair and a nondegenerate excitation. All three translational modes of H₂@ATOCF exhibit significant negative anharmonicity, which we found also in H₂@C₆₀ and H₂@C₇₀.

The angular anisotropy of the PES lifts entirely the three-fold degeneracy of the $j \rightarrow 1$ rotational level of H₂ in ATOCF, in contrast to C₆₀ where the degeneracy is left intact, or C₇₀ in which the $j \rightarrow 1$ level is partially split and shows the 1:2

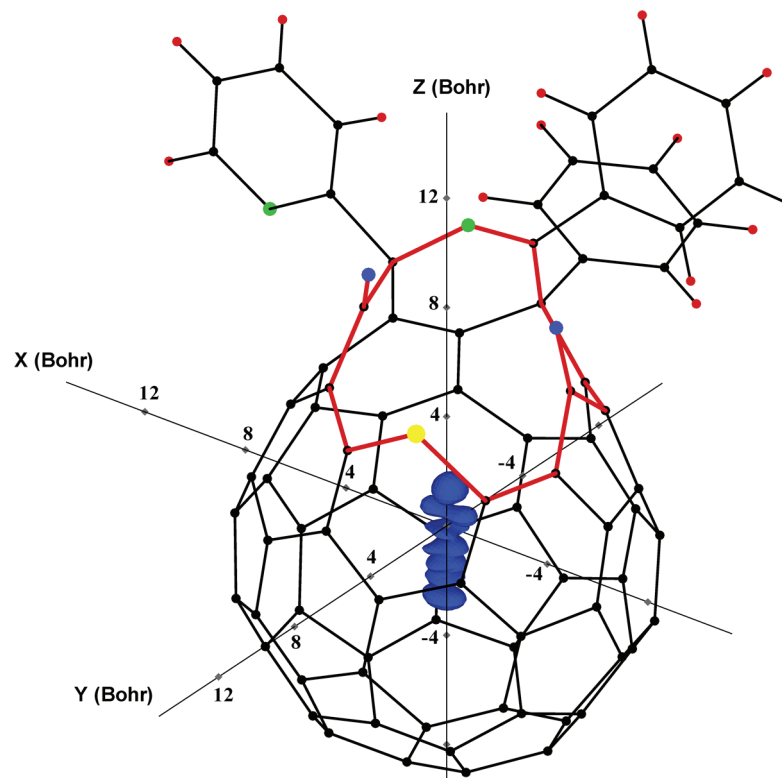


Figure 7. 3D isosurface of the reduced probability density in the translational (Cartesian) coordinates of the z -mode state $(0, 0, 6)$ of $(j = 0)$ $p\text{-H}_2$, listed in Table 2, inside ATOCF. The isosurface is drawn at 10% of the maximum value of the density.

degeneracy pattern. Translational excitation has little effect on the magnitude of the splittings of the rotational multiplets, except for the highest-frequency z -mode whose fundamental excitation increases the splitting of the $j = 1$ triplet by 70% relative to that in the translational ground state $(0, 0, 0)$.

The agreement with the INS data²⁴ for $\text{H}_2@\text{ATOCF}$ is semiquantitative. Our calculations and the experiment agree that both the $j = 1$ rotational level of the H_2 and the translational fundamental are fully split into a triplet. The $j = 1$ splitting of 17.1 cm^{-1} calculated for the ground translational state is close to the experimental value of 23.0 cm^{-1} . The remaining discrepancy of about 25% shows that angular anisotropy of the cage environment is somewhat underestimated by the PES employed. The two translational peaks that have been reported²⁴ can be confidently assigned to our z - and x -mode fundamentals, respectively. The energy calculated for the x -mode fundamental, 149.5 cm^{-1} , nearly coincides with the translational peak observed at 144.4 cm^{-1} . On the other hand, the theoretical value of the z -mode fundamental, 118.3 cm^{-1} , is 14% lower than that of the lowest-energy INS peak at 137.9 cm^{-1} . Unlike the x mode, the z -mode excitation is directed toward the orifice of ATOCF, which contains the N and S heteroatoms, and two O atoms in the immediate vicinity, and is therefore much more sensitive to the quality of the pair potentials for H_2 interacting with these atoms. The larger difference between theory and experiment in the case of the z mode implies that the two-site H_2 -heteroatom pair potentials employed are not as accurate for this system as the three-site H_2 -C pair potential. The calculated y -mode fundamental at 230.9 cm^{-1} is consistent with the estimated energy²⁴ of $230 - 240 \text{ cm}^{-1}$ for the third translation peak. In addition to the y -mode fundamental, several other calculated excitations such as $(0, 0, 2)$, $(1, 0, 1)$, and $(2, 0, 0)$, lie in the range $230 - 320 \text{ cm}^{-1}$, where a band of overlapping peaks appears in the INS spectra,²⁴ and are likely to provide at least a partial assignment of this region of the spectrum.

Our future work in this direction will include the calculation of the equilibrium constants for the encapsulation of H_2 in ATOCF based on the quantum 5D T-R energy levels, the rates of escape of the trapped H_2 , as well as the determination of more accurate H_2 -C heteroatom pair potentials by means of ab initio electronic structure calculations. In addition, we plan to study the quantum dynamics of one and two H_2 molecules in an open-cage derivative of C_{70} , which has been experimentally investigated recently.⁷

Acknowledgment. Z. B. is grateful to the National Science Foundation for partial support of this research. The computational resources used in this work were funded in part by the NSF MRI grant CHE-0420870. Acknowledgment is made to the donors of the American Chemical Society Petroleum Research Fund for partial support of this research. N. J. T. thanks the NSF for support of this research through grant CHE-0717518.

References and Notes

- (1) Rubin, Y. *Chem.s Eur. J.* **1997**, 3, 1009.
- (2) Rubin, Y. *Top. Curr. Chem.* **1999**, 199, 67.
- (3) Rubin, Y.; Jarrosson, T.; Wang, G. W.; Bartberger, M. D.; Houk, K. N.; Schick, G.; Saunders, M.; Cross, R. J. *Angew. Chem., Int. Ed.* **2001**, 40, 1543.
- (4) Murata, Y.; Murata, M.; Komatsu, K. *J. Am. Chem. Soc.* **2003**, 125, 7152.
- (5) Komatsu, K.; Murata, M.; Murata, Y. *Science* **2005**, 307, 238.
- (6) Murata, M.; Murata, Y.; Komatsu, K. *J. Am. Chem. Soc.* **2006**, 128, 8024.
- (7) Murata, Y.; Maeda, S.; Murata, M.; Komatsu, K. *J. Am. Chem. Soc.* **2008**, 130, 6702.
- (8) Murata, M.; Maeda, S.; Morinaka, Y.; Murata, Y.; Komatsu, K. *J. Am. Chem. Soc.* **2008**, 130, 15800.
- (9) Carravetta, M.; Johannessen, O. G.; Levitt, M. H.; Heinmaa, I.; Stern, R.; Samoson, A.; Horsewill, A. J.; Murata, Y.; Komatsu, K. *J. Chem. Phys.* **2006**, 124, 104507.

- (10) Carravetta, M.; Danquigny, A.; Mamone, S.; Cuda, F.; Johannessen, O. G.; Heinmaa, I.; Panesar, K.; Stern, R.; Grossel, M. C.; Horsewill, A. J.; Samoson, A.; Murata, M.; Murata, Y.; Komatsu, K.; Levitt, M. H. *Phys. Chem. Chem. Phys.* **2007**, *9*, 4879.
- (11) Sartori, E.; Ruzzi, M.; Turro, N. J.; Decatur, J. D.; Doetschman, D. C.; Lawler, R. G.; Buchachenko, A. L.; Murata, Y.; Komatsu, K. *J. Am. Chem. Soc.* **2006**, *128*, 14752.
- (12) Lopez-Gejo, J.; Marti, A. A.; Ruzzi, M.; Jockusch, S.; Komatsu, K.; Tanabe, F.; Murata, Y.; Turro, N. J. *J. Am. Chem. Soc.* **2007**, *129*, 14554.
- (13) Sartori, E.; Ruzzi, M.; Turro, N. J.; Komatsu, K.; Murata, Y.; Lawler, R. G.; Buchachenko, A. L. *J. Am. Chem. Soc.* **2008**, *130*, 2221.
- (14) Turro, N. J.; Marti, A. A.; Chen, J. Y.-C.; Jockusch, S.; Lawler, R. G.; Ruzzi, M.; Sartori, E.; Chuang, S. C.; Komatsu, K.; Murata, Y. *J. Am. Chem. Soc.* **2008**, *130*, 10506.
- (15) Turro, N. J.; Chen, J. Y.-C.; Sartori, E.; Ruzzi, M.; Marti, A.; Lawler, R.; Jockusch, S.; Lopez-Gejo, J.; Komatsu, K.; Murata, Y. *Acc. Chem. Res.* **2010**, *43*, 335.
- (16) Xu, M.; Elmatad, Y.; Sebastianelli, F.; Moskowitz, J. W.; Bačić, Z. *J. Phys. Chem. B* **2006**, *110*, 24806.
- (17) Xu, M.; Sebastianelli, F.; Bačić, Z. *J. Chem. Phys.* **2008**, *128*, 244715.
- (18) Sebastianelli, F.; Xu, M.; Bačić, Z. *J. Chem. Phys.* **2008**, *129*, 244706.
- (19) Xu, M.; Sebastianelli, F.; Bačić, Z. *J. Phys. Chem. A* **2009**, *113*, 7601.
- (20) Xu, M.; Sebastianelli, F.; Bačić, R.; Lawler, R.; Turro, N. J. *J. Chem. Phys.* **2008**, *128*, 011101.
- (21) Xu, M.; Sebastianelli, F.; Bačić, Z.; Lawler, R.; Turro, N. J. *J. Chem. Phys.* **2008**, *129*, 064313.
- (22) Mamone, S.; Ge, M.; Hivonen, D.; Nagel, U.; Danquigny, A.; Cuda, F.; Grossel, M. C.; Murata, Y.; Komatsu, K.; Levitt, M. H.; Room, T.; Carravetta, M. *J. Chem. Phys.* **2009**, *130*, 081103.
- (23) Xu, M.; Sebastianelli, F.; Gibbons, B. R.; Bačić, Z.; Lawler, R.; Turro, N. J. *J. Chem. Phys.* **2009**, *130*, 224306.
- (24) Horsewill, A. J.; Panesar, K. S.; Rols, S.; Johnson, M. R.; Murata, Y.; Komatsu, K.; Mamone, S.; Danquigny, A.; Cuda, F.; Maltsev, S.; Grossel, M. C.; Carravetta, M.; Levitt, M. H. *Phys. Rev. Lett.* **2009**, *102*, 013001.
- (25) Murata, Y.; Murata, M.; Komatsu, K. *Chem.s Eur. J.* **2003**, *9*, 1600.
- (26) Liu, S.; Bačić, Z.; Moskowitz, J. W.; Schmidt, K. E. *J. Chem. Phys.* **1995**, *103*, 1829.
- (27) Bačić, Z.; Light, J. C. *Annu. Rev. Phys. Chem.* **1989**, *40*, 469.
- (28) MacKerell, A. D.; Bashford, D.; Bellot, M.; Dunbrack, R. L.; Eveneck, J. D., Jr.; Field, M. J.; Fischer, S.; Gao, J.; Ha, S.; Joseph-McCarthy, D.; Kuchnir, L.; Kuczera, K.; Lau, F. T. K.; Mattos, C.; Michnick, S.; Ngo, T.; Nguyen, D. T.; Prothom, B.; Reiher, W. E.; Roux, III, B.; Schlenkrich, M.; Smith, J. C.; Stote, R.; Straub, J.; Watanabe, M.; Wiorkiewicz-Kuczera, J.; Yin, D.; Karplus, M. *J. Phys. Chem. B* **1998**, *102*, 3586.
- (29) Rappe, A. K.; Casewit, C. J.; Colwell, K. S.; Goddard III, W. A.; Skiff, W. M. *J. Am. Chem. Soc.* **1992**, *114*, 10024.
- (30) Mayo, S. L.; Olafson, B. D.; Goddard III, W. A. *J. Phys. Chem.* **1990**, *94*, 8897.

JP104367J